Journal of Photonics for Energy

PhotonicsforEnergy.SPIEDigitalLibrary.org

Solvent effects and charge transfer states in organic photovoltaics: a time-dependent density functional theory study on the PCPDTBT: PCBM low band gap system

Kangmin Liu
Hao Li
Sergei Tretiak
Vladimir Chernyak

SPIE.

Kangmin Liu, Hao Li, Sergei Tretiak, Vladimir Chernyak, "Solvent effects and charge transfer states in organic photovoltaics: a time-dependent density functional theory study on the PCPDTBT:PCBM low band gap system," *J. Photon. Energy* **8**(3), 032215 (2018), doi: 10.1117/1.JPE.8.032215.

Solvent effects and charge transfer states in organic photovoltaics: a time-dependent density functional theory study on the PCPDTBT:PCBM low band gap system

Kangmin Liu,[a] Hao Li,[b] Sergei Tretiak,[c] and Vladimir Chernyak[a,*]
[a]Wayne State University, Department of Chemistry, Detroit, Michigan, United States
[b]University of Houston, Department of Chemistry, Houston, Texas, United States
[c]Los Alamos National Laboratory, Los Alamos, New Mexico, United States

Abstract. Long-range corrected time-dependent density functional theory has been used to study the solvent effect on excited state properties of PCPDTBT:PCBM (Poly[2,6-(4,4-dimethyl-4H-cyclopenta[2,1-b:3,4-b′]-dithiophene)-alt-4,7-(2,1,3-benzothiadiazole)]:[6,6]-Phenyl-C61-butyric acid methyl ester) molecular system. A polarizable continuum model has been applied within the linear response (LR) and state-specific (SS) approaches to account for the dielectric environment. The results show that the influence of the solvent depends on the nature of the excitations. For neutral excitonic states that are essentially localized on a single molecule, the solvent has little or no effects on the excitation energies according to both solvent schemes. On the other hand, for states with a significant amount of charge transfer (CT), the SS approach predicts a sufficient decline in the excitation energy as the dielectric constant increases so that the CT state can be stabilized to the lowest excited state, whereas the LR counterpart shows almost no change. The comparison of two solvent approaches is discussed. © *2018 Society of Photo-Optical Instrumentation Engineers (SPIE)* [DOI: 10.1117/1.JPE.8.032215]

Keywords: organic photovoltaics; charge transfer state; solvent effect.

Paper 18016SS received Jan. 23, 2018; accepted for publication Apr. 20, 2018; published online May 21, 2018.

1 Introduction

Charge transfer (CT) is one of the most important processes in a variety of photochemical, photophysical, and biological phenomena.[1] In the process of light-to-electricity conversion occurring in organic solar cells, such as bulk heterojunction (BHJ) devices, excitons are created by absorbing photons in the electron donor domain and diffuse to the heterojunction interface to dissociate into free charges. Although intensive research effort has been made, the mechanism of free charge generation in BHJs is still unclear. More research suggests that interfacial charge transfer states (CTSs) play a significant role in the generation of free photocarriers. These states are also involved in singlet fission processes, thus providing a possible way to increase the conversion efficiency.[2] It has been proposed that high-lying singlet states, i.e., hot excitons, could directly convert to hot interfacial CTSs that immediately yield free charge carriers[3,4] due to the excessive energy. On the other hand, there are experimental results[5,6] suggesting that vibrationally equilibrated or cold CTSs could also serve as precursors of free polarons. In addition, the results of transient absorption spectroscopy reveal that the electric field generated by interfacial CTSs may affect the optical transitions in the surrounding molecules and cause ultrafast free charge generation.[7] We also notice other works such as the observation of polaronic signature within 100 fs but no further relaxation in the resonance Raman spectroscopy, which suggests direct exciton dissociation into free charges.[8] The mechanism of the resonant tunneling for delocalized

*Address all correspondence to: Vladimir Chernyak, E-mail: chernyak@chem.wayne.edu

1947-7988/2018/$25.00 © 2018 SPIE

excitons in the presence of strong vibronic coupling may also facilitate the ultrafast long-range charge separation.[9–11] Nevertheless, the CTS is a crucial factor in ultrafast charge separation processes in BHJ materials and deserves substantial research attention.

Electronic excitations in a multichromophoric system such as conjugated polymers are usually tightly bound excitons that are numerically difficult to characterize due to their many body nature. Compared with silicon semiconductors, the low dimensionality (quasione-dimensional or two-dimensional) and low relative permittivity of organic conjugated molecules strengthen the electron-hole interaction and result in relatively small exciton size and large exciton binding energy that cannot be perturbatively treated. Such a fact further complicates the theoretical simulation on the corresponding excited-state processes. Another difficulty in excited-state simulations comes from the interaction between the reacting molecular system and its surrounding polarizable media such as a solvent or solid-state matrix. Due to the difference in electrostatic dipole between excitations such as intermolecular CTSs and intramolecular excitations, quantitative modeling of the excited-state energetic alignment is a nontrivial computational task that requires methods not only to account for the aforementioned strong excitonic effect, but also to correctly model the polarizable environment with respect to the excitation.

Among all the OPV materials, BHJ devices composed of polymeric electron donors and fullerene-based electron acceptors have gained enormous attention due to their high-power conversion efficiency, low cost, and many technological advantages.[12,13] The PCPDTBT:PCBM pair shown in Fig. 1 represents a promising BHJ family of a low band gap copolymer system because of the high charge mobility, good processability, optimal band gap of the PCPDTBT molecule, and the outstanding solubility of PCBM.[14–16] Although the excited-state properties of these materials have been studied by a variety of theoretical methods,[3,17,18] detailed investigation into solvent effects on electronic transitions is still lacking. The potentially strong dipole–dipole interaction between the BHJ matter and its surrounding medium may considerably affect excited-state properties and likewise the generation of free charges. Therefore, we performed quantum-chemical simulations to illustrate how the nearby dielectric environment affects electronic excitations, in particular CTSs, in BHJ complexes.

In this article, we conducted a computational investigation into the relation between the solvent polarity and the excited-state energetic alignment in an organic BHJ complex commonly used in photovoltaic devices within a range-corrected time-dependent density functional theory (TDDFT) framework. We begin with a brief overview of computational techniques for the

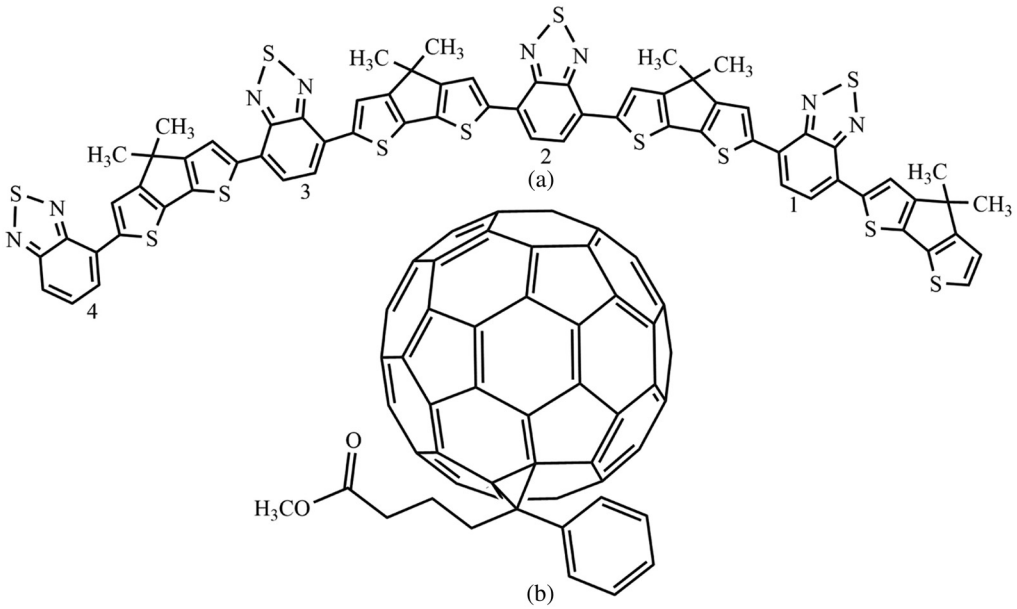

Fig. 1 Chemical structures of (a) poly[2,6-(4,4-dimethyl-4H-cyclopenta[2,1-b:3,4-b′]-dithiophene)-alt-4,7-(2,1,3-benzothiadiazole)] (PCPDTBT) and (b) [6,6]-Phenyl-C61-butyric acid methyl ester ($PC_{61}BM$).

prototype molecular complex in Sec. 2 and the computational details are specified in Sec. 3. The results are discussed in Sec. 4 regarding the calculation in vacuo and in solvent with varying dielectric constant. Our conclusions are summarized in Sec. 5.

2 Overview of Computational Methods

Generally in organic photovoltaics, the exciton binding energy and electron–hole separation lie between those of Frenkel excitons[19] and Wannier–Mott excitons.[20] Therefore, both excitonic and CT characters may exist simultaneously in the photoexcitations of conjugated compounds and such a fact further complicates the description of the corresponding electronic structures.[21–25] An intermolecular CT state is formed with prominent charge displacement between neighboring molecules and often followed by strong Stark effect due to its large electric dipole moment. In contrast, an excitonic (EX) state is associated with limited charge movement and the electron and hole are relatively tightly bounded. Therefore, one can formally distinguish a CT state from EX states by examining the static dipole moments. However, the EX and CT characters often coexist in one excitation with varying degrees of mixing. Examination of the corresponding transition density matrix (to be specified in Sec. 3) provides a more accurate estimate of the CT characters for a given excited state.

In the past two decades, TDDFT has become a routine technique for excited-state computation because of its favorable accuracy-to-cost ratio. In the Kohn–Sham (KS) formalism, the Schrödinger equation in terms of noninteracting electron density can be solved by the self-consistent field method with the approximate exchange-correlation (XC) functional representing molecular Hamiltonian. The linear response TDDFT based on Casida's formulation has been widely used to compute electronic excitations and is programmed in a variety of electronic structure codes.[26] However, in case of the strong excitonic effect in conjugated structures, the TDDFT method often fails to predict excitonic effects,[27–29] the energies of CT excitations,[30,31] as well as material band gaps and chemical reaction barriers.[32] Improvements can be achieved by introducing the charge/spin constraints on the electronic density obeying chemical intuition such as the constrained DFT method.[33–35]

An alternative way to eliminate the delocalization error in XC functionals is to adopt hybrid functionals that involve nonlocal exchange potential with range separation.[36,37] CAM-B3LYP,[38] ω97X,[39] and screened range-separated hybrid (SRSH)[40] are examples of long-range-corrected models, where the exchange potentials at short and long ranges are separately approximated.

The other concern in the simulation of CTS comes from the interaction between the reacting molecular system and its surrounding polarizable media such as a solvent or solid state. The environmental polarization can alter the excited-state electronic structure of the solute and vice versa.[41] In organic semiconductors, the CTSs are notably sensitive to the nearby solvent polarization because of their large electrostatic dipoles.[42,43] The CT excitations in solution may be computed by adopting basic continuum models, where the solvent is a continuum dielectric hosting the solute in a cavity.[35] An example of such an approach is the LR-TDDFT method, which, however, often underestimates the CT energy correction because the solvent polarization is evaluated from the transition density rather than the excited-state density.[44–46] One way to address this deficiency is the so-called state-specific (SS) solvation approach, in which the correction on the transition energy is computed by making the excited-state density self-consistent with the corresponding solvent polarization. As shown in previous studies,[46–50] the SS approach is generally reliable to determine energy correction associated with the charge redistribution of the solute upon the electronic transition.

The van der Waals interactions between molecules are essential in determining molecular structures and conformations for large molecules and aggregates.[51,52] A prevalent way to account for these interactions is to add empirical dispersion corrections to the underlying functional. Popular models include Petersson–Frisch[53] and Grimme's[54–56] models, which are reliable to use together with a variety of XC functionals when computing large molecular systems.

Considering all aforementioned factors, a lot of studies on the CT transitions in organic semiconductors have been conducted using different techniques. For example, the energetics of CT excitations at organic interfaces has been calculated based on SRSH functional.[57] This study

demonstrated agreement with the experimental values for the CTS energies of the donor/acceptor complexes of pentacene with C60 and poly-3-hexylthiophene (P3HT) with PCBM. Zheng and coworkers[35] have developed several protocols to compute CT state energies for conjugated molecules in polar solvent. By employing the Baer–Neuhauser–Livshits (BNL) functional and polarizable continuum model (PCM) for solvent effect in the constrained DFT method, they showed that solvation can considerably affect the CTS energies. This observation successfully explained the enhanced red-shift between the absorption and emission spectra of stilbene-functionalized octahedral silsesquioxanes.[58] A similar protocol reproduces also the solvated CTS energies for a series of functionalized anthracene and tetracyanoethylene dimers.[35] Nieman et al.[59] employed TDDFT with range-corrected CAM-B3LYP functional to simulate the CTSs in fullerenes:P3HT complex separated by aligned oligothiophenes. Combined with experimental studies, their work revealed that the CT process can be facilitated by the dielectric environment. In this article, we investigated the CTS properties in another widely used BHJ family PCPDTBT:PCBM complex with respect to solvent polarity, for the first time to the best of our knowledge, under the range-corrected DFT framework.

3 Computational Details

Here we focus on the low-lying electronic singlet states in the BHJ complex of PCPDTBT:PCBM. Detailed ab initio simulations on dynamical processes in real BHJ aggregates are currently numerically forbidden due to the large dimension of the system and the complexity arising from the configuration of the mixture. Therefore, in this work, we simplify the donor–acceptor interface as a molecular model that consists of a tetramer of the donor oligomer and a single buckyball. Such a simplified model allows extensive numerical simulations by probing the effects of several density functionals, geometries, and a broad range of dielectric constants, thus delivering detailed information on the solvent effect on the energy-level alignment. Because the optical band gap in PCPDTBT tends to saturate for oligomers with four repeat units,[15,17] PCPDTBT tetramer is selected to minimize the numerical cost and retain the essential physics of interest. Our computational model is an approximation to the experimental polymer: fullerene blend: it neglects the effects of intramolecular delocalizations beyond the oligomer length, geometrical conformations due to solid-state packing, and the effects of intermolecular interactions with neighboring polymers and fullerenes that may also perturb the excited state alignment. The lowest 20 vertical excitations for the oligomer, the buckyball, and their complex have been calculated both in vacuo and in solvent environment with varying static dielectric constant using the DFT/TDDFT method. The density of states of the excitonic states in the individual PCPDTBT and PCBM have been calculated, respectively, whereas the CT character for the intermolecular CT excitations has been evaluated from the calculation of the dimers.

LC hybrid functionals CAM-B3LYP[38] and ωB97XD[60] have been employed together with 6-31G(d) basis set for both ground-state structure optimizations and excited-state calculations. The 6-31G(d) basis was shown to be sufficient in the simulations of BHJ systems in the comparison with larger cc-pVTZ basis.[35] The Coulomb-attenuating method is used in CAM-B3LYP functional to modulate the fraction orbital exchange in the XC functional within the range of 19% to 65%. To describe intermolecular dispersion interactions binding the dimer, Grimme's dispersion correction has been applied together with CAM-B3LYP functional to the DFT-D2 and DFT-D3 levels,[55,56] hereafter referred to as GD2 and GD3. Compared with CAM-B3LYP, the ωB97XD functional includes more orbital exchange varying from 22% to 100%. In addition, the empirical dispersion correction is already built in ωB97XD functional.

We optimized the ground-state geometries of both PCPDTBT and PCBM monomers in vacuo using the three functional models. Then, the optimized monomer structures were combined together by placing the fullerene above the center of the PCPDTBT molecule. Being specific, the initial complex is oriented such that the center of PCBM is aligned with the second benzothiadiazole segment with the closest interatomic distance of 3.1 Å, whereas the side group of PCBM is placed away from PCPDTBT to minimize the steric hindrance. The complex of PCPDTBT:PCBM was subject to further ground-state optimization in vacuo with the

respective functionals. Different initial dimer configurations have been approached with the consideration of maximizing the $\pi - \pi$ stacking and minimizing the steric hindrance, so that we could find the global optimal structures. The simulation in solution was performed using PCM[44] with varying dielectric constant. First, we have evaluated the solvent effect on excited states at the LR TDDFT level.[61] Here the calculations do not require the excited-state density explicitly, thus avoiding significant numerical cost.[47] We further performed the excited-state computation based on the SS approach,[50] in which the effective solvent potential directly depends on the excited state density.

In case of vertical excitation, the nonequilibrium solvation procedure associated with fast solvent response requires optical dielectric constants in addition to the static counterpart. Both factors are involved in nonequilibrium solvation, but only the latter one is responsible for equilibrium states. Solvent permittivity including optical dielectric constant (ε_∞) and static dielectric constant (ε_r) can be specified for different solvents and solvation scenarios. As the dominant solvent effect comes from the static dielectric constant of the solvent, in this work, we focus on the solvent effect of static dielectric constant and leave the frequency-dependent optical one for future study. Specifically, in all simulations the optical dielectric constant was fixed to $\varepsilon_\infty = 2.0$ close to that of dichloromethane, whereas ε_r was allowed to vary in the range of $3 < \varepsilon_r < 30$. All calculations were conducted with Gaussian 09 computational package.[62]

We distinguish the intermolecular CT states from ordinary excitonic states by employing the so-called CT factor, which can be obtained by averaging over the respective matrix elements of the transition density matrix.[51,63] The CT factor ranging from 0 to 1 represents completely localized excitation on a single molecule and CT transition, respectively. In the present work, we define excitations with CT factors >0.9 as intermolecular CT states, <0.1 as EX states, and the transitions with $0.1 < \mathrm{CT} < 0.9$ are referred to as hybrid states.[52] We focus on the energetics of the lowest CT state denoted by CT-1 and the lowest two EX states (EX-1 and EX-2), track how the solvent dielectric environment affects the CT character, and visualize the electronic excitations using the natural transition orbitals (NTOs)[64] and contour plots of the transition density matrices.[65]

4 Results and Discussion

Using optimal ground-state geometries for PCPDTBT, PCBM, and their complex, we computed 20 excited states in vacuo and in solvent with varied ε_r. Obtained excitation energies, oscillator strengths, transition density matrices, and NTO analysis are detailed in Appendix A. We particularly focus on the lowest two excitonic states (EX-1,2) and the lowest CT state (CT-1).

4.1 *Electronic Excitations in Vacuo*

The simulated stick absorption spectra for 15 lowest states of PCPDTBT, PCBM, and the complex of PCPDTBT:PCBM computed in vacuo are shown in Fig. 2. Detailed excited-state data including evaluated CT factors are tabulated in Tables 1–3 in Appendix A.

The spectra for the monomers calculated at the three TDDFT levels agree very well with each other in terms of both excitation energy and oscillator strength. As expected, the multiple excited states in PCPDTBT oligomer are optically allowed such as the lowest energy band-gap transition, which corresponds to the peak at 725 nm in its UV–Vis absorption spectrum associated with the $S_0 \rightarrow S_1$ transition.[15] In contrast, almost all excitations in the PCBM are optically forbidden due to the high symmetry of the molecule.

To analyze and compare the EX/CT character in the complex, we visualized the excitations of interest using the respective NTOs and contour plots of the transition density matrices as shown in Figs. 3, 4, and 6–8 in Appendix A. First, we notice that the lowest two excited states EX-1 and EX-2 in the complex are associated with the oligomer with their transition energies only slightly perturbed by the presence of the fullerene. Indeed, the lowest excitation is limited within the PCPDTBT moiety but delocalized over the entire oligomer, whereas the second excitation can be represented by the NTOs pairs, each involving half of the oligomer chain (Fig. 6).

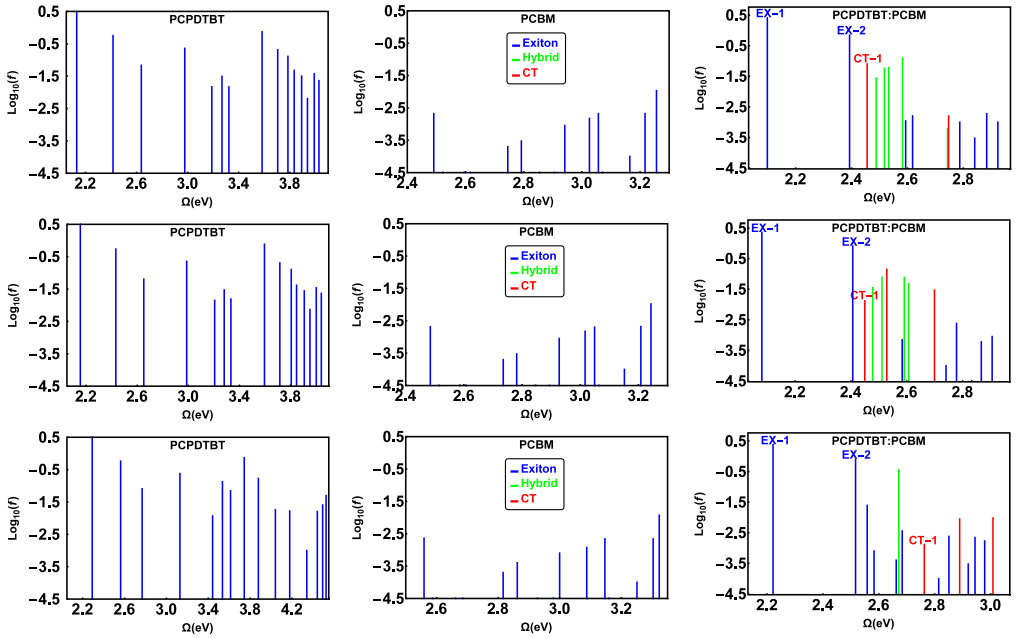

Fig. 2 Stick absorption spectra of PCPDTBT, PCBM, and PCPDTBT:PCBM complex (from left to right) in vacuo computed at CAM-B3LYP/GD3 (top row), CAM-B3LYP/GD2 (middle row), and ωB97XD (bottom row). The *x*-axis denotes transition energies Ω, whereas the *y*-axis denotes $\mathrm{Log}_{10}(f)$, *f* being unitless oscillator strength of a given transition. States are color-coded according to the CT factor, i.e., blue for EX states with CT $\leq$ 0.1, green for hybrid states with 0.1 < CT < 0.9, and red for CT states with CT $\geq$ 0.9.

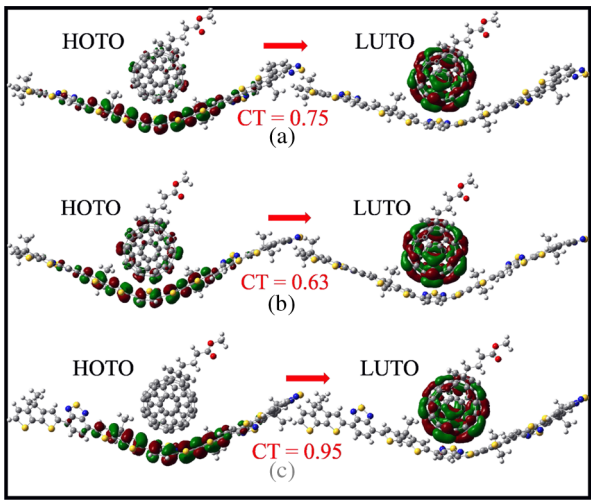

Fig. 3 Visualization of NTOs of the lowest CT state with the highest occupied transition orbital (HOTO) on the left and the lowest unoccupied transition orbital (LUTO) on the right computed at (a) CAM-B3LYP/GD3, (b) CAM-B3LYP/GD2, and (c) ωB97XD. The associated eigenvalues λ are 0.91, 0.92, and 0.97, respectively, which represents the weights of the particle-hole pair contributes to the excitation.

This observation may be interpreted by the symmetry of the exciton wave function.[66] The CT transitions in a complex appear at much larger energies. Namely, the lowest observed CT state from the ωB97XD calculation has slightly higher transition energy and a stronger CT character than those obtained from CAM-B3LYP levels. Specifically, the lowest CT state in ωB97XD calculation corresponds to the eighth excited state with CT = 0.95, whereas CT-1 obtained from CAM-B3LYP is attributed to the third excitation and CT = 0.63 and 0.75 for GD2 and GD3 levels, respectively. The NTO representation in Fig. 3 qualitatively agrees with the

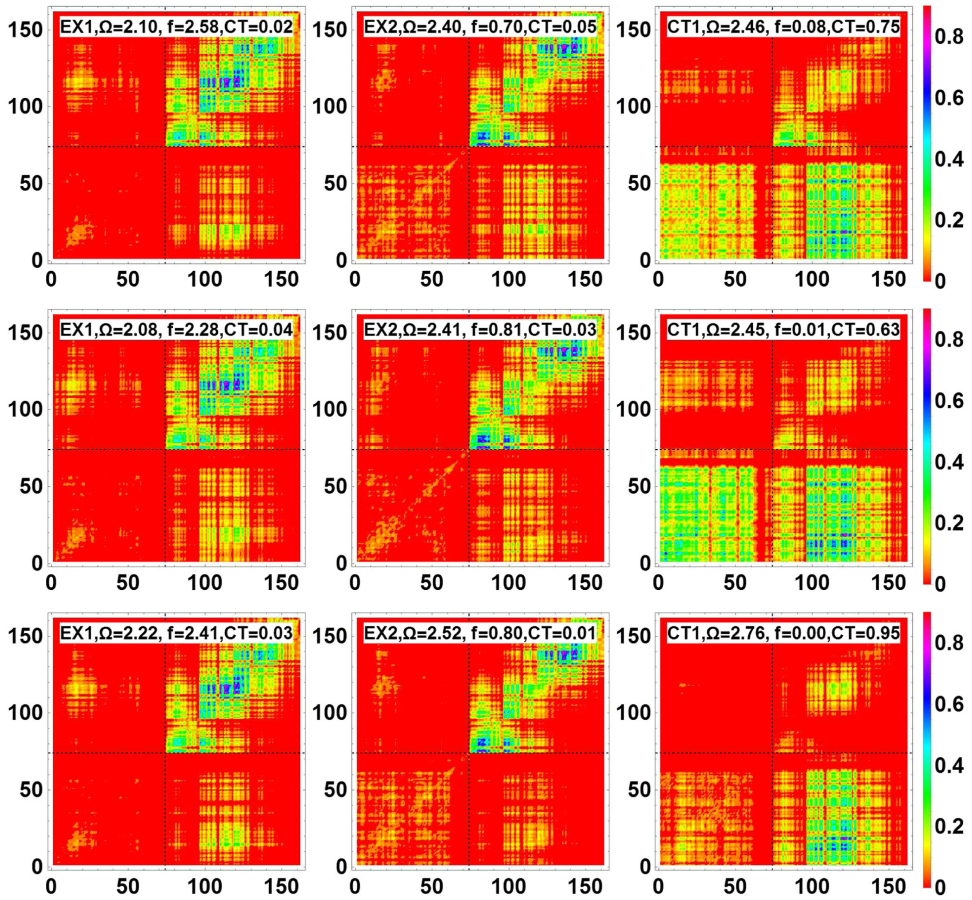

Fig. 4 The lowest two excited states EX-1,2 and the lowest charge transfer state CT-1 of PCPDTBT:PCBM in vacuo given by contour plots of the transition density matrices from the ground state to excited states, obtained by (a) CAM-B3LYP/GD3/6-31G(d), (b) CAM-B3LYP/GD2/6-31G(d), and (c) ωB97XD/6-31G(d). The axis labels represent indices of nonhydrogen atoms from PCBM to PCPDTBT (PCBM: 1–74, PCPDTBT: 75–162). The inset of each plot shows the character of the electronic mode, excitation energy Ω, oscillator strength *f*, and the CT factor.

CT factors evaluated from the transition densities, e.g., CT-1 in ωB97XD carries more CT character, whereas the one determined from CAM-B3LYP/GD2 has the least. The two-dimensional contour plots (Fig. 4) of the transition density matrix for dimer states can be roughly interpreted as a 2×2 block matrix, in which the diagonal elements represent the excitation happening within each monomer, whereas the off-diagonal blocks indicate that the excitation transfers a charge from one moiety to the other. This representation already suggests a weak hybridization of the excitonic and CT character for all states in question. Thus, both the visualized NTOs and the contour plots of the transition density matrices confirm that excited states EX-1,2 occur in the oligomer moiety, whereas in the CT-1 state electrons are driven from PCPDTBT to the fullerene moiety.

4.2 *Electronic Excitations in Solvent*

We have singled out the states of our interest, EX-1,2 and CT-1, from the simulation in vacuo by examining the excitation nature and evaluating the CT factor. Here, we expose the PCPDTBT:PCBM dimer to the polarizable solvent environment with varied static dielectric constant, so that the solvent effect on electronic transitions may be illustrated. Both LR and SS solvations have been performed for all the simulations.

The dependence of transition energies for the states of interest of PCPDTBT:PCBM complex on the solvent polarity is shown in Fig. 5. Note that in the panels of the upper row,

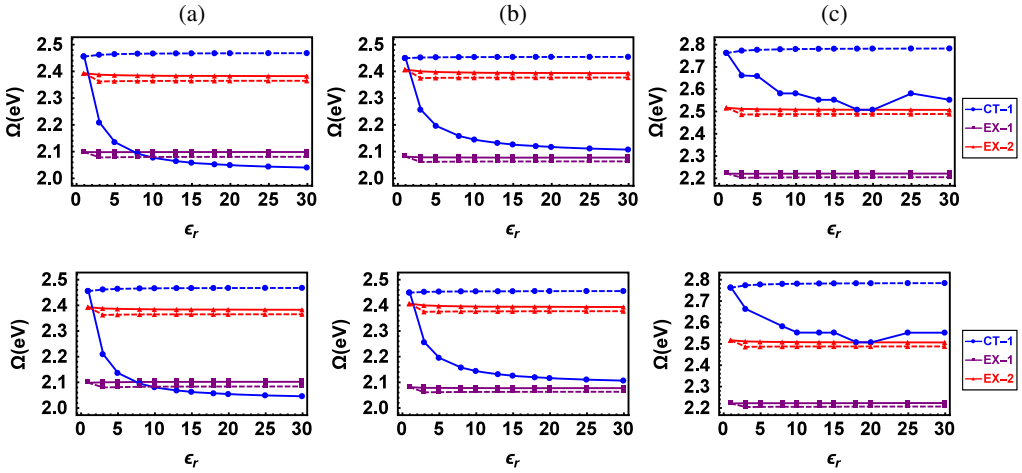

Fig. 5 Comparison of excited state calculation in solvent based on vacuum geometry (first row) and solvated geometry (second row), computed at (a) CAM-B3LYP/GD3, (b) CAM-B3LYP/GD2, and (c) ωB97XD. For the solvated calculations, each PCPDTBT:PCBM ground state geometry is optimized in the presence of solvent with the corresponding dielectric constant.

the calculations use the ground-state geometries optimized in vacuo, whereas the lower panels show the results obtained with the ground-state geometries optimized in the presence of solvent with different dielectric constants. Detailed numerical results including excitation energy, oscillator strength, and CT factor can be found in Tables 4–9 in Appendices B and C. Comparison of these results indicates that further geometrical optimization is not necessary because the molecular configuration is essentially determined by the dispersive interactions and only weakly depends on the solvent. In the low-cost LR simulations, the solvatochromic shift (i.e., excitation energy difference between gas phase and solution) is small, and the solvent polarity has a little or no effect on all excitations. Overall, we observe variations in energies due to solvent within 0.01 eV for both excitonic and CT states in all three levels of simulations. Such weak solvent effect can be attributed to the LR approach in which the solvatochromic shift is computed from transition density, which tends to be small. More importantly, the CT factor of CT-1 state considerably diminishes with respect to the dielectric constant in CAM-B3LYP simulations, whereas the CT factors of EX-1,2 states are relatively stable (Fig. 9 in Appendix D). Such observation being opposed to physical intuition encourages us to adopt the more reliable SS approach. Here, a very significant decrease in the CT-1 energy (up to 0.4 eV) has been observed in all simulations using the SS solvation approach. In cases of CAM-B3LYP computation, the CT energy saturates when $\varepsilon_r \geq 13$, which can be easily found in common polar solvent. In addition, the CT factor of CT-1 state increases (0.95 in CAM-B3LYP) compared with the gas phase results (0.6 to 0.7). As expected, the solvent effects simulated by the SS approach are much less pronounced for the excitonic states EX-1,2 either in excitation energy or in the CT factor. Because the polar solvent affects the CT and EX states in different ways, we observed the different alignments of energetics. In CAM-B3LYP/GD3 calculation, the CT state, being the third excitation in gas phase, becomes the second excited state in low polarity case and becomes the lowest one when $\varepsilon_r \geq 8$. In other words, strong polar solvent can stabilize polarizable excitations by much larger solvatochromic shift and induce more polarized feature to the states. In the case of ωB97XD computations, a similar trend of energy change due to ε_r is observed, although the decrease in CT-1 energy (<0.3 eV) is not as significant as those in CAM-B3LYP calculations. The CT factors of both excitonic and CT states are insensitive to the change in ε_r for both LR and SS approaches.

The noticeable difference in the CTS stabilization between the three computational levels is essentially attributed to the different range-corrected properties taken into account in the functionals. As mentioned in Sec. 3, more fraction of orbital exchange included in ωB97XD functional indicates less delocalized electron effect. Therefore, we observed less CTS

stabilization due to the solvent effect as a direct result of weaker CT character in ωB97XD simulation compared with CAM-B3LYP counterparts. In addition, the difference in the dispersion correction results in different dimer configurations, in particular, the distance between the two molecules. We noticed that the separation between PCPDTBT and PCBM in ωB97XD simulation (≈3.12 Å) is slightly further than those in CAM-B3LYP calculations (≈3.09 Å), whereas the difference of distance between CAM-B3LYP simulations at GD2 and GD3 levels is >0.01 Å. Such observation follows an obvious fact that the intermolecular CTSs are very sensitive to the molecular distance and less likely to form in case of larger separation.

The high internal quantum efficiency of charge separation is routinely achieved in the devices with PCPDTBT:PCBM mixture. This suggests that CT states are generally energetically favorable compared with the excitonic counterparts. In our simulations, we observe that CT-1 becomes lower than EX-1 only for a single modeling approach (CAM-B3LYP/GD3) for larger than the experimental value of the dielectric constant. Such observed under-stabilization of CT states is due to multiple effects. We have already discussed above sensitivity of CT state on the dispersion corrections and long-range-corrected model implementation in the DFT functional. It has been studied that neighboring chromophores also play an important role in the CTS stabilization. The enhanced red-shift of emissive CTS in silsesquioxane derivatives can be interpreted as the strong CT character between chromophores as well as the solvent effect.[58] Such enhanced CTS stabilization has also been illustrated in the TDDFT simulation of P3HT:C_{60} complex with oligothiophene spacer. Significant energy drop in CTS has been obtained in the BHJ complex spaced by three π-stacking oligomers compared with the counterpart with a single oligomer spacer.[59] Generally, more chromophores result in a higher degree of π-electron delocalization and hence possibly stronger CT character, which makes the state more stable in the concern of solvent effect. Considering the heterogeneous distribution of donor and acceptor in real BHJ materials, the CTS stabilization due to the solvent effect observed in the simplified molecular dimer will be enhanced taking into account the nearby chromophores. In addition, the electric field generated by interfacial charges in BHJ mixture may act similar as polar solvent does to further facilitate the formation of CT state by lowering its energy and optimize the overall power conversion efficiency.[7] Finally, vibrational stabilization of polar CT state is larger than neutral EX state, which may further facilitate energetic stabilization and formation of spatially separated polarons.

5 Conclusion

In this work, we have conducted a TDDFT investigation on how the solvent polarity affects the electronic excitations in the representative organic BHJ PCPDTBT:PCBM simplified as a molecular dimer. Range-corrected hybrid functionals CAM-B3LYP and ωB97XD have been used along with the dispersion correction within the empirical Grimme's models to account for weak intermolecular interactions. Two prevalent solvation approaches, the LR and SS approaches, have been applied and compared. Little-to-no solvent effect on the solute energetics and CT character has been observed from the result in the LR scheme, whereas the solvent effect is pronounced in the SS simulation in line with experimental observations and common physical sense. Being specific, the intermolecular CT state with large polarization is more sensitive to polar solvent than the homogeneous excitations, and such an effect is well simulated within the SS scheme. Based on the analysis of the NTOs and CT factors, we conclude that solvent with larger dielectric constant can lower the CT energy and aggravate the CT character but has little effect on the excitations with less charge redistribution.

In summary, the TDDFT method that combines long-range-corrected hybrid functional, dispersion correction, and a state-specific solvation model provides an efficient and correct approach to simulate the excited-state electronic structure in organic BHJ systems. We demonstrated the detailed characterization of CTS stabilization due to the polar solvent environment within the TDDFT framework for the first time for the representative PCPDTBT:PCBM system.

Appendix A: Excited State Calculations in Vacuo

We performed excited electronic structure calculations with three functional models. In Appendix A, we provide the results of the calculations in vacuo. The NTOs for EX-1, 2 are shown in Figs. 6–8, and the excitation energies and oscillator strength for the first 15 excited states of PCPDTBT, PCBM, and PCPDTBT:PCBM are included in Tables 1–3, which correspond to the results calculated with the functional CAM-B3LYP/GD3/6-31G(d), CAM-B3LYP/GD2/6-31G(d), and ωB97XD/6-31G(d), respectively.

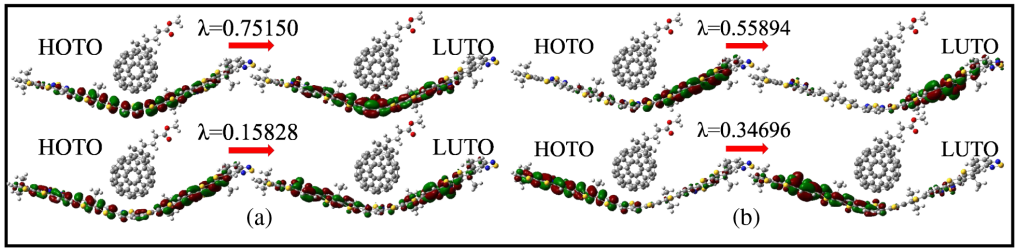

Fig. 6 NTOs of (a) EX-1 and (b) EX-2 states, both have two major contributing pairs, λ is the associated eigenvalue that represents the weights of the particle-hole pair contributes to the excitation. The HOTO and the LUTO are labeled. Computed by CAM-B3LYP/GD3/6-31G(d) in vacuo.

Table 1 Excitation energies and oscillator strength of PCPDTBT, PCBM and PCPDTBT:PCBM in vacuo. CT factors for PCPDTBT:PCBM are listed. *D* stands for donor and *A* for acceptor, DA-charge transfer from donor to acceptor, DD-charge localization within donor. Computed by CAM-B3LYP/6-31G(d) on the ground-state geometry optimized by the same functional with the empirical dispersion correction GD3.

CAM-B3LYP-GD3/6-31G(d) geometry in vacuo									
	PCPDTBT		PCBM		PCPDTBT:PCBM				
Mode	$\Omega(eV)$	f	$\Omega(eV)$	f	$\Omega(eV)$	f	CT(DA)	DD	AA
1	2.13	3.38	2.49	0.00	2.10	2.58	0.02	0.97	0.00
2	2.42	0.56	2.52	0.00	2.39	0.70	0.05	0.94	0.01
3	2.64	0.07	2.59	0.00	2.46	0.08	0.75	0.08	0.17
4	2.98	0.23	2.62	0.00	2.49	0.03	0.29	0.03	0.68
5	3.19	0.01	2.75	0.00	2.52	0.06	0.33	0.11	0.55
6	3.27	0.03	2.79	0.00	2.53	0.06	0.28	0.14	0.58
7	3.32	0.01	2.85	0.00	2.58	0.13	0.46	0.48	0.06
8	3.58	0.74	2.91	0.00	2.59	0.00	0.00	0.00	0.99
9	3.71	0.21	2.94	0.00	2.62	0.00	0.04	0.01	0.95
10	3.79	0.13	3.03	0.00	2.74	0.00	0.15	0.06	0.79
11	3.83	0.05	3.06	0.00	2.75	0.00	0.56	0.20	0.24
12	3.89	0.03	3.07	0.00	2.79	0.00	0.03	0.00	0.96
13	3.94	0.01	3.16	0.00	2.84	0.00	0.01	0.00	0.99
14	3.99	0.04	3.22	0.00	2.88	0.00	0.02	0.01	0.97
15	4.03	0.02	3.26	0.01	2.92	0.00	0.01	0.00	0.98

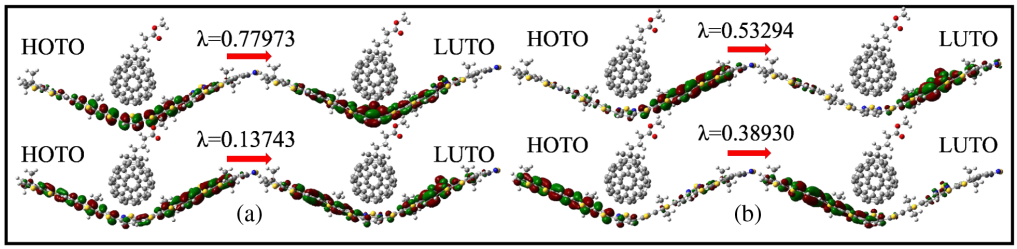

Fig. 7 NTOs of (a) EX-1 and (b) EX-2 states, both have two major contributing pairs, λ is the associated eigenvalue which represents the weights of the particle-hole pair contributes to the excitation. The HOTO and the LUTO are labeled. Computed by CAM-B3LYP/GD2/6-31G(d) in vacuo.

Table 2 Excitation energies and oscillator strength of PCPDTBT, PCBM and PCPDTBT:PCBM in Vacuo. CT factors for PCPDTBT:PCBM are listed. Computed by CAM-B3LYP/6-31G(d) on the ground state geometry optimized by the same functional with the empirical dispersion correction GD2.

CAM-B3LYP-GD2/6-31G(d) in vacuo									
	PCPDTBT		PCBM		PCPDTBT:PCBM				
Mode	$\Omega(eV)$	f	$\Omega(eV)$	f	$\Omega(eV)$	f	CT(DA)	DD	AA
1	2.15	3.39	2.48	0.00	2.08	2.28	0.04	0.96	0.00
2	2.43	0.54	2.51	0.00	2.41	0.81	0.03	0.97	0.00
3	2.65	0.06	2.59	0.00	2.45	0.01	0.63	0.02	0.35
4	2.99	0.23	2.61	0.00	2.48	0.04	0.23	0.03	0.74
5	3.21	0.01	2.74	0.00	2.51	0.08	0.17	0.09	0.74
6	3.28	0.03	2.78	0.00	2.53	0.14	0.60	0.20	0.19
7	3.33	0.02	2.85	0.00	2.58	0.00	0.01	0.00	0.99
8	3.60	0.77	2.89	0.00	2.59	0.08	0.15	0.30	0.55
9	3.72	0.20	2.93	0.00	2.61	0.05	0.29	0.26	0.44
10	3.81	0.13	3.02	0.00	2.70	0.03	0.74	0.20	0.06
11	3.85	0.04	3.05	0.00	2.74	0.00	0.01	0.00	0.98
12	3.91	0.03	3.06	0.00	2.78	0.00	0.03	0.00	0.95
13	3.95	0.01	3.15	0.00	2.83	0.00	0.02	0.00	0.97
14	4.00	0.03	3.21	0.00	2.87	0.00	0.02	0.01	0.96
15	4.04	0.02	3.24	0.01	2.91	0.00	0.02	0.00	0.97

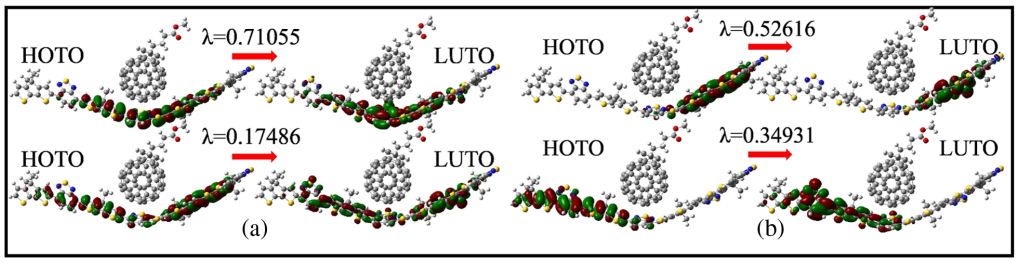

Fig. 8 NTOs of (a) EX-1 and (b) EX-2 states, both have two major contributing pairs, λ is the associated eigenvalue which represents the weights of the particle-hole pair contributes to the excitation. The HOTO and the LUTO are labeled. Computed by ωB97XD/6-31G(d) in vacuo.

Table 3 Excitation energies and oscillator strength of PCPDTBT, PCBM and PCPDTBT:PCBM in vacuo. CT factors for PCPDTBT:PCBM are listed. Computed by ωB97XD/6-31G(d) on the ground state geometry optimized by the same functional.

ωB97XD/6-31G(d) in vacuo									
	PCPDTBT		PCBM		PCPDTBT:PCBM				
Mode	$\Omega(eV)$	f	$\Omega(eV)$	f	$\Omega(eV)$	f	CT(DA)	DD	AA
1	2.29	3.38	2.56	0.00	2.22	2.41	0.03	0.97	0.00
2	2.56	0.57	2.59	0.00	2.52	0.80	0.01	0.98	0.01
3	2.77	0.08	2.66	0.00	2.56	0.02	0.01	0.01	0.98
4	3.13	0.24	2.69	0.00	2.58	0.00	0.01	0.00	0.99
5	3.44	0.01	2.82	0.00	2.66	0.00	0.00	0.00	0.99
6	3.53	0.13	2.86	0.00	2.67	0.36	0.16	0.81	0.02
7	3.61	0.07	2.93	0.00	2.68	0.00	0.00	0.01	0.98
8	3.74	0.74	2.98	0.00	2.76	0.00	0.95	0.02	0.03
9	3.88	0.17	3.00	0.00	2.81	0.00	0.01	0.00	0.99
10	4.04	0.02	3.09	0.00	2.85	0.00	0.05	0.01	0.94
11	4.18	0.02	3.15	0.00	2.89	0.01	0.79	0.11	0.11
12	4.34	0.00	3.16	0.00	2.92	0.00	0.01	0.00	0.98
13	4.44	0.02	3.25	0.00	2.94	0.00	0.07	0.00	0.92
14	4.49	0.03	3.30	0.00	2.98	0.00	0.08	0.01	0.90
15	4.52	0.05	3.32	0.01	3.01	0.01	0.77	0.11	0.12

Appendix B: Excited State Calculations in Solvent Based on Vacuum Geometries

In Appendix B, we provide the results of the calculations in solvent based on the geometries optimized in vacuo. Tables 4–6 correspond to functional CAM-B3LYP/6-31G(d) + GD3, CAM-B3LYP/6-31G(d) + GD2, and ωB97XD/6-31G(d), respectively. In each table, the excitation energy, oscillator strength, CT factor of EX-1, 2 and CT-1 in solvent with different polarity are shown with two solvent approaches, LR and SS.

Table 4 Excitation energies, Ω, oscillator strength, f, and CT factors of the molecular pair of PCPDTBT:PCBM in solvent with varying static dielectric constant, ε. Three modes are of the main concern, the first two excitonic states (EX-1,2) and the charge transfer state (CT-1). Computed by CAM-B3LYP/6-31G(d) using the LR and the SS approaches on the geometry optimized by the same functional with the empirical dispersion correction GD3.

CAM-B3LYP-GD3/6-31G(d) PCPDTBT:PCBM in solvent with vacuum geometry											
		LR					SS				
ε_r	mode	$\Omega(eV)$	f	CT(DA)	DD	AA	$\Omega(eV)$	f	CT(DA)	DD	AA
1	EX-1	2.10	2.58	0.02	0.97	0.00	2.10	2.58	0.02	0.97	0.00
	EX-2	2.39	0.70	0.05	0.94	0.01	2.39	0.70	0.05	0.94	0.01
	CT-1	2.46	0.08	0.75	0.08	0.17	2.46	0.08	0.75	0.08	0.17

Table 4 (*Continued*).

CAM-B3LYP-GD3/6-31G(d) PCPDTBT:PCBM in solvent with vacuum geometry

		LR					SS				
ε_r	mode	$\Omega(eV)$	f	CT(DA)	DD	AA	$\Omega(eV)$	f	CT(DA)	DD	AA
3	EX-1	2.08	2.72	0.02	0.98	0.00	2.10	2.57	0.02	0.97	0.00
	EX-2	2.36	0.81	0.02	0.97	0.00	2.39	0.70	0.04	0.95	0.01
	CT-1	2.46	0.08	0.65	0.08	0.28	2.21	0.05	0.95	0.03	0.01
5	EX-1	2.08	2.73	0.02	0.98	0.00	2.10	2.57	0.02	0.97	0.00
	EX-2	2.36	0.81	0.02	0.97	0.00	2.39	0.70	0.04	0.96	0.01
	CT-1	2.46	0.08	0.60	0.08	0.32	2.14	0.07	0.96	0.03	0.01
8	EX-1	2.08	2.73	0.02	0.98	0.00	2.10	2.56	0.02	0.97	0.00
	EX-2	2.36	0.81	0.02	0.97	0.00	2.38	0.70	0.03	0.96	0.01
	CT-1	2.47	0.08	0.57	0.08	0.36	2.09	0.09	0.96	0.03	0.01
10	EX-1	2.08	2.73	0.02	0.98	0.00	2.10	2.56	0.02	0.97	0.00
	EX-2	2.36	0.81	0.02	0.97	0.00	2.38	0.70	0.03	0.96	0.01
	CT-1	2.47	0.08	0.55	0.08	0.37	2.08	0.10	0.96	0.04	0.01
13	EX-1	2.08	2.73	0.02	0.98	0.00	2.10	2.56	0.02	0.97	0.00
	EX-2	2.36	0.81	0.02	0.97	0.00	2.38	0.70	0.03	0.96	0.01
	CT-1	2.47	0.08	0.54	0.08	0.38	2.06	0.11	0.95	0.04	0.01
15	EX-1	2.08	2.73	0.02	0.98	0.00	2.10	2.56	0.02	0.97	0.00
	EX-2	2.36	0.81	0.02	0.97	0.00	2.38	0.70	0.03	0.96	0.01
	CT-1	2.47	0.08	0.54	0.08	0.39	2.06	0.12	0.95	0.04	0.01
18	EX-1	2.08	2.73	0.02	0.98	0.00	2.10	2.56	0.02	0.97	0.00
	EX-2	2.36	0.81	0.02	0.97	0.00	2.38	0.70	0.03	0.96	0.01
	CT-1	2.47	0.08	0.53	0.08	0.39	2.05	0.12	0.95	0.04	0.01
20	EX-1	2.08	2.73	0.02	0.00	0.00	2.10	2.56	0.02	0.97	0.00
	EX-2	2.36	0.81	0.02	0.00	0.00	2.38	0.70	0.03	0.96	0.01
	CT-1	2.47	0.08	0.53	0.00	0.40	2.05	0.13	0.95	0.04	0.01
25	EX-1	2.08	2.73	0.02	0.98	0.00	2.10	2.56	0.02	0.97	0.00
	EX-2	2.36	0.81	0.02	0.97	0.00	2.38	0.70	0.03	0.96	0.01
	CT-1	2.47	0.08	0.52	0.08	0.40	2.04	0.14	0.95	0.05	0.01
30	EX-1	2.08	2.73	0.02	0.98	0.00	2.10	2.56	0.02	0.97	0.00
	EX-2	2.36	0.81	0.02	0.97	0.00	2.38	0.70	0.03	0.96	0.01
	CT-1	2.47	0.08	0.52	0.08	0.41	2.04	0.14	0.94	0.05	0.01

Table 5 Excitation energies, Ω, oscillator strength, *f*, and CT factors of the molecular pair of PCPDTBT:PCBM in solvent with varying static dielectric constant, ε. Three modes are of the main concern, the first two excitonic states (EX-1,2) and the charge transfer state (CT-1). Computed by CAM-B3LYP/6-31G(d) using the LR and the SS approaches on the geometry optimized by the same functional with the empirical dispersion correction GD2.

CAM-B3LYP-GD2/6-31G(d) PCPDTBT:PCBM in solvent with vacuum geometry											
		LR					SS				
ε_r	Mode	$\Omega(eV)$	*f*	CT(DA)	DD	AA	$\Omega(eV)$	*f*	CT(DA)	DD	AA
1	EX-1	2.08	2.28	0.04	0.96	0.00	2.08	2.28	0.04	0.96	0.00
	EX-2	2.41	0.81	0.03	0.97	0.00	2.41	0.81	0.03	0.97	0.00
	CT-1	2.45	0.01	0.63	0.02	0.35	2.45	0.01	0.63	0.02	0.35
3	EX-1	2.06	2.41	0.03	0.96	0.00	2.08	2.26	0.04	0.96	0.00
	EX-2	2.37	0.91	0.02	0.98	0.00	2.40	0.81	0.03	0.97	0.00
	CT-1	2.45	0.01	0.56	0.02	0.42	2.26	0.04	0.94	0.02	0.03
5	EX-1	2.06	2.41	0.03	0.96	0.00	2.08	2.26	0.04	0.96	0.00
	EX-2	2.38	0.91	0.02	0.98	0.00	2.40	0.80	0.03	0.97	0.00
	CT-1	2.45	0.01	0.54	0.01	0.45	2.20	0.05	0.95	0.02	0.03
8	EX-1	2.06	2.42	0.03	0.96	0.00	2.08	2.25	0.04	0.96	0.00
	EX-2	2.38	0.92	0.02	0.98	0.00	2.40	0.80	0.02	0.97	0.00
	CT-1	2.45	0.01	0.52	0.01	0.47	2.16	0.06	0.95	0.03	0.02
10	EX-1	2.06	2.42	0.03	0.96	0.00	2.08	2.25	0.04	0.96	0.00
	EX-2	2.38	0.92	0.02	0.98	0.00	2.40	0.80	0.02	0.97	0.00
	CT-1	2.45	0.01	0.51	0.01	0.47	2.14	0.07	0.95	0.03	0.02
13	EX-1	2.06	2.42	0.03	0.96	0.00	2.08	2.25	0.04	0.96	0.00
	EX-2	2.38	0.92	0.02	0.98	0.00	2.39	0.80	0.02	0.97	0.00
	CT-1	2.45	0.01	0.50	0.01	0.48	2.13	0.07	0.95	0.03	0.02
15	EX-1	2.06	2.42	0.03	0.96	0.00	2.08	2.25	0.04	0.96	0.00
	EX-2	2.38	0.92	0.02	0.98	0.00	2.39	0.80	0.02	0.97	0.00
	CT-1	2.45	0.01	0.50	0.01	0.48	2.13	0.07	0.95	0.03	0.02
18	EX-1	2.06	2.42	0.03	0.96	0.00	2.08	2.25	0.04	0.96	0.00
	EX-2	2.38	0.92	0.02	0.98	0.00	2.39	0.80	0.02	0.97	0.00
	CT-1	2.45	0.01	0.50	0.01	0.49	2.12	0.08	0.95	0.03	0.02
20	EX-1	2.06	2.42	0.03	0.96	0.00	2.08	2.25	0.04	0.96	0.00
	EX-2	2.38	0.92	0.02	0.98	0.00	2.39	0.80	0.02	0.97	0.00
	CT-1	2.45	0.01	0.50	0.01	0.49	2.12	0.08	0.95	0.03	0.02
25	EX-1	2.06	2.42	0.03	0.96	0.00	2.08	2.25	0.04	0.96	0.00
	EX-2	2.38	0.92	0.02	0.98	0.00	2.39	0.80	0.02	0.97	0.00
	CT-1	2.45	0.01	0.49	0.01	0.49	2.11	0.08	0.95	0.03	0.02
30	EX-1	2.06	2.42	0.03	0.96	0.00	2.08	2.25	0.04	0.96	0.00
	EX-2	2.38	0.92	0.02	0.98	0.00	2.39	0.80	0.02	0.97	0.00
	CT-1	2.45	0.01	0.49	0.01	0.49	2.11	0.08	0.95	0.03	0.02

Table 6 Excitation energies, Ω, Oscillator strength, *f*, and CT factors of the molecular pair of PCPDTBT:PCBM in solvent with varying static dielectric constant, ε. Three modes are of the main concern, the first two excitonic states (EX-1,2) and the charge transfer state (CT-1). Computed by ωB97XD/6-31G(d) using the LR and the SS approaches on the geometry optimized by the same functional.

ωB97XD/6-31G(d) PCPDTBT:PCBM in solvent with vacuum geometry											
		LR					SS				
ε_r	Mode	$\Omega(eV)$	*f*	CT(DA)	DD	AA	$\Omega(eV)$	*f*	CT(DA)	DD	AA
1	EX-1	2.22	2.41	0.03	0.97	0.00	2.22	2.41	0.03	0.97	0.00
	EX-2	2.52	0.80	0.01	0.98	0.01	2.52	0.80	0.01	0.98	0.01
	CT-1	2.76	0.00	0.95	0.02	0.03	2.76	0.00	0.95	0.02	0.03
3	EX-1	2.20	2.55	0.03	0.97	0.00	2.22	2.40	0.03	0.97	0.00
	EX-2	2.49	0.90	0.01	0.99	0.00	2.51	0.79	0.01	0.98	0.01
	CT-1	2.77	0.00	0.94	0.02	0.03	2.66	0.00	0.95	0.02	0.03
5	EX-1	2.20	2.55	0.03	0.97	0.00	2.22	2.40	0.03	0.97	0.00
	EX-2	2.49	0.90	0.01	0.99	0.00	2.51	0.79	0.01	0.98	0.01
	CT-1	2.78	0.00	0.94	0.02	0.04	2.66	0.00	0.95	0.03	0.03
8	EX-1	2.20	2.56	0.03	0.97	0.00	2.22	2.40	0.03	0.97	0.00
	EX-2	2.49	0.90	0.01	0.99	0.00	2.51	0.79	0.01	0.98	0.01
	CT-1	2.78	0.00	0.94	0.02	0.04	2.58	0.00	0.94	0.02	0.04
10	EX-1	2.20	2.56	0.03	0.97	0.00	2.22	2.40	0.03	0.97	0.00
	EX-2	2.49	0.90	0.01	0.99	0.00	2.51	0.79	0.01	0.98	0.01
	CT-1	2.78	0.00	0.94	0.02	0.04	2.58	0.00	0.94	0.02	0.04
13	EX-1	2.20	2.56	0.03	0.97	0.00	2.22	2.40	0.03	0.97	0.00
	EX-2	2.49	0.90	0.01	0.99	0.00	2.51	0.79	0.01	0.98	0.01
	CT-1	2.78	0.00	0.94	0.02	0.04	2.55	0.00	0.94	0.02	0.04
15	EX-1	2.20	2.56	0.03	0.97	0.00	2.22	2.40	0.03	0.97	0.00
	EX-2	2.49	0.90	0.01	0.99	0.00	2.51	0.79	0.01	0.98	0.01
	CT-1	2.78	0.00	0.94	0.02	0.04	2.55	0.00	0.94	0.02	0.04
18	EX-1	2.20	2.56	0.03	0.97	0.00	2.22	2.40	0.03	0.97	0.00
	EX-2	2.49	0.90	0.01	0.99	0.00	2.50	0.79	0.01	0.98	0.01
	CT-1	2.78	0.00	0.94	0.02	0.04	2.50	0.00	0.94	0.02	0.04
20	EX-1	2.20	2.56	0.03	0.97	0.00	2.22	2.40	0.03	0.97	0.00
	EX-2	2.49	0.90	0.01	0.99	0.00	2.50	0.79	0.01	0.98	0.01
	CT-1	2.78	0.00	0.94	0.02	0.04	2.50	0.00	0.94	0.02	0.04
25	EX-1	2.21	2.56	0.03	0.97	0.00	2.22	2.40	0.03	0.97	0.00
	EX-2	2.49	0.90	0.01	0.99	0.00	2.50	0.79	0.01	0.98	0.01
	CT-1	2.78	0.00	0.94	0.02	0.04	2.58	0.00	0.94	0.02	0.04
30	EX-1	2.21	2.56	0.03	0.97	0.00	2.22	2.40	0.03	0.97	0.00
	EX-2	2.49	0.90	0.01	0.99	0.00	2.50	0.79	0.01	0.98	0.01
	CT-1	2.78	0.00	0.94	0.02	0.04	2.55	0.00	0.94	0.02	0.04

Appendix C: Excited State Calculations in Solvent Based on Solvated Geometries

The previous section examines the electronic properties based on vacuum geometries. In Appendix C, we provide the results of the calculations in solvent based on solvated geometries. Tables 7–9 correspond to functional CAM-B3LYP/6-31G(d) + GD3, CAM-B3LYP/6-31G(d) + GD2, and ωB97XD/6-31G(d), respectively. In each table, the excitation energy, oscillator strength, CT factor of EX-1, 2 and CT-1 in solvent with different polarity are shown with two solvent approaches, LR and SS.

Table 7 Excitation energies, Ω, oscillator strength, *f*, and CT factors of the molecular pair of PCPDTBT:PCBM in solvent with varying static dielectric constant, ε. Three modes are of the main concern, the first two excitonic states (EX-1,2) and the charge transfer state (CT-1). Computed by CAM-B3LYP/6-31G(d) using the LR and the SS approaches on the geometry optimized by the same functional with the empirical dispersion correction GD3.

CAM-B3LYP-GD3/6-31G(d) PCPDTBT:PCBM in solvent with solvated geometry											
		LR					SS				
ε_r	Mode	$\Omega(eV)$	*f*	CT(DA)	DD	AA	$\Omega(eV)$	*f*	CT(DA)	DD	AA
1	EX-1	2.10	2.58	0.02	0.97	0.00	2.10	2.58	0.02	0.97	0.00
	EX-2	2.39	0.70	0.05	0.94	0.01	2.39	0.70	0.05	0.94	0.01
	CT-1	2.46	0.08	0.75	0.08	0.17	2.46	0.08	0.75	0.08	0.17
3	EX-1	2.08	2.72	0.02	0.98	0.00	2.10	2.58	0.02	0.97	0.00
	EX-2	2.36	0.81	0.02	0.97	0.00	2.39	0.69	0.04	0.95	0.01
	CT-1	2.46	0.08	0.63	0.08	0.29	2.21	0.06	0.95	0.03	0.01
5	EX-1	2.08	2.73	0.02	0.98	0.00	2.10	2.58	0.02	0.97	0.00
	EX-2	2.36	0.81	0.02	0.97	0.00	2.39	0.69	0.04	0.96	0.01
	CT-1	2.46	0.08	0.58	0.08	0.34	2.14	0.08	0.96	0.03	0.01
8	EX-1	2.08	2.73	0.02	0.98	0.00	2.10	2.59	0.02	0.97	0.00
	EX-2	2.36	0.81	0.02	0.97	0.00	2.38	0.68	0.03	0.96	0.01
	CT-1	2.47	0.08	0.54	0.08	0.38	2.09	0.10	0.95	0.04	0.01
10	EX-1	2.08	2.73	0.02	0.98	0.00	2.10	2.59	0.02	0.97	0.00
	EX-2	2.36	0.81	0.02	0.97	0.00	2.38	0.68	0.03	0.96	0.01
	CT-1	2.47	0.08	0.53	0.08	0.39	2.08	0.12	0.95	0.04	0.01
13	EX-1	2.08	2.73	0.02	0.98	0.00	2.10	2.59	0.02	0.97	0.00
	EX-2	2.36	0.81	0.02	0.97	0.00	2.38	0.68	0.03	0.96	0.01
	CT-1	2.47	0.08	0.51	0.08	0.41	2.07	0.13	0.95	0.05	0.01
15	EX-1	2.08	2.73	0.02	0.98	0.00	2.10	2.59	0.02	0.97	0.00
	EX-2	2.36	0.81	0.02	0.97	0.00	2.38	0.68	0.03	0.96	0.01
	CT-1	2.47	0.08	0.51	0.08	0.41	2.06	0.14	0.94	0.05	0.01
18	EX-1	2.08	2.73	0.02	0.98	0.00	2.10	2.59	0.02	0.97	0.00
	EX-2	2.37	0.81	0.02	0.97	0.00	2.38	0.68	0.03	0.96	0.01
	CT-1	2.47	0.08	0.50	0.08	0.42	2.06	0.15	0.94	0.05	0.01

Table 7 (*Continued*).

CAM-B3LYP-GD3/6-31G(d) PCPDTBT:PCBM in solvent with solvated geometry											
		LR					SS				
ε_r	Mode	$\Omega(eV)$	f	CT(DA)	DD	AA	$\Omega(eV)$	f	CT(DA)	DD	AA
20	EX-1	2.08	2.73	0.02	0.98	0.00	2.10	2.59	0.02	0.97	0.00
	EX-2	2.37	0.81	0.02	0.97	0.00	2.38	0.68	0.03	0.96	0.01
	CT-1	2.47	0.08	0.50	0.08	0.42	2.05	0.15	0.94	0.05	0.01
25	EX-1	2.08	2.73	0.02	0.98	0.00	2.10	2.59	0.02	0.97	0.00
	EX-2	2.37	0.81	0.02	0.97	0.00	2.38	0.68	0.03	0.96	0.01
	CT-1	2.47	0.08	0.49	0.08	0.43	2.05	0.16	0.94	0.05	0.01
30	EX-1	2.08	2.73	0.02	0.98	0.00	2.10	2.59	0.02	0.97	0.00
	EX-2	2.37	0.81	0.02	0.97	0.00	2.38	0.68	0.03	0.96	0.01
	CT-1	2.47	0.08	0.49	0.08	0.43	2.05	0.17	0.94	0.06	0.01

Table 8 Excitation energies, Ω, oscillator strength, f, and CT factors of the molecular pair of PCPDTBT:PCBM in solvent with varying static dielectric constant, ε. Three modes are of the main concern, the first two excitonic states (EX-1,2) and the charge transfer state (CT-1). Computed by CAM-B3LYP/6-31G(d) using the LR and the SS approaches on the geometry optimized by the same functional with the empirical dispersion correction GD2.

CAM-B3LYP-GD2/6-31G(d) PCPDTBT:PCBM in solvent with solvated geometry											
		LR					SS				
ε_r	Mode	$\Omega(eV)$	f	CT(DA)	DD	AA	$\Omega(eV)$	f	CT(DA)	DD	AA
1	EX-1	2.08	2.28	0.04	0.96	0.00	2.08	2.28	0.04	0.96	0.00
	EX-2	2.41	0.81	0.03	0.97	0.00	2.41	0.81	0.03	0.97	0.00
	CT-1	2.45	0.01	0.63	0.02	0.35	2.45	0.01	0.63	0.02	0.35
3	EX-1	2.06	2.42	0.03	0.96	0.00	2.08	2.27	0.04	0.96	0.00
	EX-2	2.37	0.91	0.02	0.98	0.00	2.40	0.80	0.03	0.97	0.00
	CT-1	2.45	0.01	0.57	0.02	0.41	2.26	0.05	0.95	0.02	0.03
5	EX-1	2.06	2.42	0.03	0.96	0.00	2.08	2.27	0.04	0.96	0.00
	EX-2	2.38	0.91	0.02	0.98	0.00	2.40	0.80	0.03	0.97	0.00
	CT-1	2.45	0.01	0.54	0.02	0.44	2.20	0.06	0.95	0.02	0.02
8	EX-1	2.06	2.43	0.03	0.96	0.00	2.08	2.26	0.04	0.96	0.00
	EX-2	2.38	0.91	0.02	0.98	0.00	2.40	0.79	0.02	0.97	0.00
	CT-1	2.45	0.01	0.52	0.01	0.47	2.16	0.07	0.95	0.03	0.02
10	EX-1	2.06	2.43	0.03	0.96	0.00	2.08	2.26	0.04	0.96	0.00
	EX-2	2.38	0.91	0.02	0.98	0.00	2.40	0.79	0.02	0.97	0.00
	CT-1	2.45	0.01	0.51	0.01	0.47	2.14	0.07	0.95	0.03	0.02

Table 8 (*Continued*).

CAM-B3LYP-GD2/6-31G(d) PCPDTBT:PCBM in solvent with solvated geometry

		LR					SS				
ε_r	Mode	$\Omega(eV)$	f	CT(DA)	DD	AA	$\Omega(eV)$	f	CT(DA)	DD	AA
13	EX-1	2.06	2.43	0.03	0.96	0.00	2.08	2.26	0.04	0.96	0.00
	EX-2	2.38	0.91	0.02	0.98	0.00	2.39	0.79	0.02	0.97	0.00
	CT-1	2.45	0.01	0.50	0.01	0.48	2.13	0.07	0.95	0.03	0.02
15	EX-1	2.06	2.43	0.03	0.96	0.00	2.08	2.26	0.04	0.96	0.00
	EX-2	2.38	0.91	0.02	0.98	0.00	2.39	0.79	0.02	0.97	0.00
	CT-1	2.45	0.01	0.50	0.01	0.48	2.13	0.08	0.95	0.03	0.02
18	EX-1	2.06	2.43	0.03	0.96	0.00	2.08	2.26	0.04	0.96	0.00
	EX-2	2.38	0.90	0.02	0.98	0.00	2.39	0.79	0.02	0.97	0.00
	CT-1	2.46	0.01	0.50	0.01	0.48	2.12	0.08	0.95	0.03	0.02
20	EX-1	2.06	2.43	0.03	0.96	0.00	2.08	2.26	0.04	0.96	0.00
	EX-2	2.38	0.90	0.02	0.98	0.00	2.39	0.79	0.02	0.97	0.00
	CT-1	2.46	0.01	0.50	0.01	0.48	2.12	0.08	0.95	0.03	0.02
25	EX-1	2.06	2.43	0.03	0.96	0.00	2.08	2.26	0.04	0.96	0.00
	EX-2	2.38	0.90	0.02	0.98	0.00	2.39	0.79	0.02	0.97	0.00
	CT-1	2.46	0.01	0.50	0.01	0.49	2.11	0.09	0.95	0.03	0.02
30	EX-1	2.06	2.43	0.03	0.96	0.00	2.08	2.26	0.04	0.96	0.00
	EX-2	2.38	0.90	0.02	0.98	0.00	2.39	0.79	0.02	0.97	0.00
	CT-1	2.46	0.01	0.50	0.01	0.49	2.11	0.09	0.95	0.03	0.02

Table 9 Excitation energies, Ω, oscillator strength, f, and CT factors of the molecular pair of PCPDTBT:PCBM in solvent with varying static dielectric constant, ε. Three modes are of the main concern, the first two excitonic states (EX-1,2) and the charge transfer state (CT-1). Computed by ωB97XD/6-31G(d) using the LR and the SS approaches on the geometry optimized by the same functional.

ωB97XD/6-31G(d) PCPDTBT:PCBM in solvent with solvated geometry

		LR					SS				
ε_r	Mode	$\Omega(eV)$	f	CT(DA)	DD	AA	$\Omega(eV)$	f	CT(DA)	DD	AA
1	EX-1	2.22	2.41	0.03	0.97	0.00	2.22	2.41	0.03	0.97	0.00
	EX-2	2.52	0.80	0.01	0.98	0.01	2.52	0.80	0.01	0.98	0.01
	CT-1	2.76	0.00	0.95	0.02	0.03	2.76	0.00	0.95	0.02	0.03
3	EX-1	2.20	2.57	0.03	0.97	0.00	2.22	2.42	0.03	0.97	0.00
	EX-2	2.49	0.90	0.01	0.99	0.00	2.51	0.79	0.01	0.98	0.01
	CT-1	2.77	0.00	0.95	0.02	0.03	2.66	0.00	0.95	0.02	0.03

Table 9 (*Continued*).

ωB97XD/6-31G(d) PCPDTBT:PCBM in solvent with solvated geometry

		LR					SS				
ε_r	Mode	$\Omega(eV)$	f	CT(DA)	DD	AA	$\Omega(eV)$	f	CT(DA)	DD	AA
5	EX-1	2.21	2.57	0.03	0.97	0.00	2.22	2.41	0.03	0.97	0.00
	EX-2	2.49	0.90	0.01	0.99	0.00	2.51	0.79	0.01	0.98	0.01
	CT-1	2.78	0.00	0.95	0.02	0.04					
8	EX-1	2.21	2.57	0.03	0.97	0.00	2.22	2.41	0.03	0.97	0.00
	EX-2	2.49	0.90	0.01	0.99	0.00	2.51	0.79	0.01	0.98	0.01
	CT-1	2.78	0.00	0.95	0.02	0.04	2.58	0.00	0.94	0.02	0.04
10	EX-1	2.21	2.57	0.03	0.97	0.00	2.22	2.41	0.03	0.97	0.00
	EX-2	2.49	0.90	0.01	0.99	0.00	2.51	0.78	0.01	0.98	0.01
	CT-1	2.78	0.00	0.94	0.02	0.04	2.55	0.00	0.94	0.02	0.04
13	EX-1	2.21	2.57	0.03	0.97	0.00	2.22	2.41	0.03	0.97	0.00
	EX-2	2.49	0.90	0.01	0.99	0.00	2.51	0.78	0.01	0.98	0.01
	CT-1	2.78	0.00	0.94	0.02	0.04	2.55	0.00	0.94	0.02	0.04
15	EX-1	2.21	2.57	0.03	0.97	0.00	2.22	2.41	0.03	0.97	0.00
	EX-2	2.49	0.90	0.01	0.99	0.00	2.51	0.78	0.01	0.98	0.01
	CT-1	2.78	0.00	0.94	0.02	0.04	2.55	0.00	0.94	0.02	0.04
18	EX-1	2.21	2.58	0.03	0.97	0.00	2.22	2.41	0.03	0.97	0.00
	EX-2	2.49	0.90	0.01	0.99	0.00	2.51	0.78	0.01	0.98	0.01
	CT-1	2.78	0.00	0.94	0.02	0.04	2.51	0.00	0.94	0.02	0.04
20	EX-1	2.21	2.58	0.03	0.97	0.00	2.22	2.41	0.03	0.97	0.00
	EX-2	2.49	0.90	0.01	0.99	0.00	2.51	0.78	0.01	0.98	0.01
	CT-1	2.78	0.00	0.94	0.02	0.04	2.51	0.00	0.94	0.02	0.04
25	EX-1	2.21	2.58	0.03	0.97	0.00	2.22	2.41	0.03	0.97	0.00
	EX-2	2.49	0.90	0.01	0.99	0.00	2.51	0.78	0.01	0.98	0.01
	CT-1	2.78	0.00	0.94	0.02	0.04	2.55	0.00	0.94	0.02	0.04
30	EX-1	2.21	2.58	0.03	0.97	0.00	2.22	2.41	0.03	0.97	0.00
	EX-2	2.49	0.90	0.01	0.99	0.00	2.51	0.78	0.01	0.98	0.01
	CT-1	2.78	0.00	0.94	0.02	0.04	2.55	0.00	0.94	0.02	0.04

Appendix D: Comparison of Excited State Calculations in Solvent Based on Vacuum Geometry and Solvated Geometry

To further examine the solvent effect on the excited electronic properties, we obtained the optimized geometries both in vacuo and in solvent, and then we calculated the CT factor for three excited states EX-1, 2 and CT-1 in solvent environment with varying dielectric constant. In Fig. 9, the first row represents the results based on the vacuum geometries, and the second

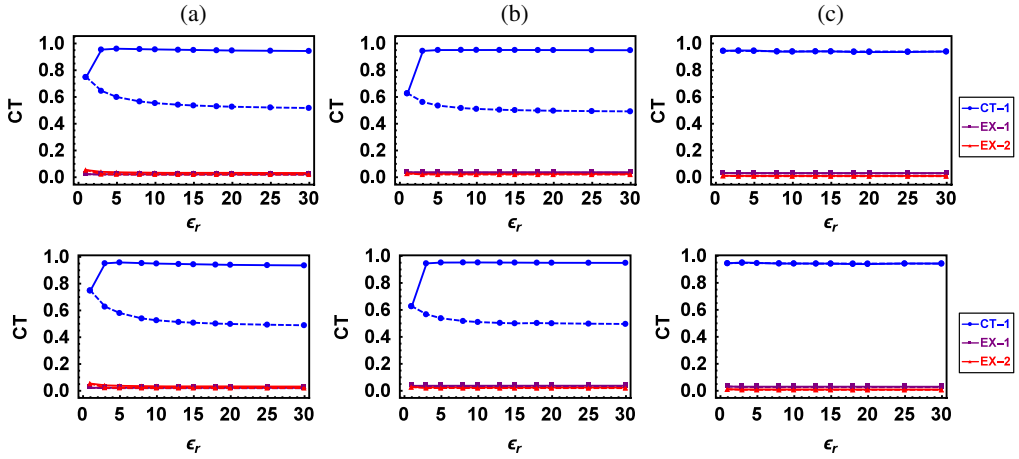

Fig. 9 CT factor of interested states with respect to the dielectric constant of the solvent. Solid and dashed curves represent SS and LR approaches, respectively. Computed at (a) CAM-B3LYP/GD3, (b) CAM-B3LYP/GD2, and (c) ωB97XD based on the ground geometries optimized in vacuo (first row) and in solvent (second row).

row is the calculations for solvated geometries. Three columns, (a), (b), (c) correspond to the three functionals, CAM-B3LYP/6-31G(d) + GD3, CAM-B3LYP/6-31G(d) + GD2, and ωB97XD/6-31G(d), respectively.

Disclosures

The authors declare no competing financial interest.

Acknowledgments

This material was based upon work supported by the National Science Foundation under Grant No. CHE- 1111350. K.L. and V.C. acknowledge support from the Chemistry Department at Wayne State University. This work was performed in part at the Center for Integrated Nanotechnologies, a U.S. Department of Energy, Office of Science user facility at Los Alamos National Laboratory (LANL). K.L also acknowledges the computational administration provided by Grid Computing Team at Wayne State University. H.L. acknowledges the support from the National Science Foundation (CHE-1664971 and MRI-1531814).

References

1. K. V. Mikkelsen and M. A. Ratner, "Electron tunneling in solid-state electron-transfer reactions," *Chem. Rev.* **87**(1), 113–153 (1987).
2. E. A. Margulies et al., "Direct observation of a charge-transfer state preceding high-yield singlet fission in terrylenediimide thin films," *J. Am. Chem. Soc.* **139**, 663–671 (2017).
3. G. Grancini et al., "Hot exciton dissociation in polymer solar cells," *Nat. Mater.* **12**, 29–33 (2013).
4. R. Volpi et al., "Theoretical study of the charge-transfer state separation within Marcus theory: the C_{60}-anthracene case study," *ACS Appl. Mater. Interfaces* **8**(37), 24722–24736 (2016).
5. K. Vandewal et al., "Efficient charge generation by relaxed charge-transfer states at organic interfaces," *Nat. Mater.* **13**, 63–68 (2014).
6. J. Lee et al., "Charge transfer state versus hot exciton dissociation in polymer-fullerene blended solar cells," *J. Am. Chem. Soc.* **132**, 11878–11880 (2010).
7. S. Gélinas et al., "Ultrafast long-range charge separation in organic semiconductor photovoltaic diodes," *Science* **343**(6170), 512–516 (2014).

8. F. Provencher et al., "Direct observation of ultrafast long-range charge separation at polymer-fullerene heterojunctions," *Nat. Commun.* **5**, 4288 (2014).
9. C. A. Rozzi et al., "Quantum coherence controls the charge separation in a prototypical artificial light-harvesting system," *Nat. Commun.* **4**, 1602 (2013).
10. S. M. Falke et al., "Coherent ultrafast charge transfer in an organic photovoltaic blend," *Science* **344**(6187), 1001–1005 (2014).
11. E. R. Bittner and C. Silva, "Noise-induced quantum coherence drives photo-carrier generation dynamics at polymeric semiconductor heterojunctions," *Nat. Commun.* **5**, 3119 (2014).
12. H. Kang et al., "Bulk-heterojunction organic solar cells: five core technologies for their commercialization," *Adv. Mater.* **28**(36), 7821–7861 (2016).
13. R. P. Singh and O. S. Kushwaha, "Polymer solar cells: an overview," *Macromol. Symp.* **327**(1), 128–149 (2013).
14. J. Peet et al., "Efficiency enhancement in low-bandgap polymer solar cells by processing with alkane dithiols," *Nat. Mater.* **6**, 497–500 (2007).
15. D. Fazzi et al., "Ultrafast internal conversion in a low band gap polymer for photovoltaics: experimental and theoretical study," *Phys. Chem. Chem. Phys.* **14**, 6367–6374 (2012).
16. G. Grancini et al., "Influence of blend composition on ultrafast charge generation and recombination dynamics in low band gap polymer-based organic photovoltaics," *J. Phys. Chem. C* **116**, 9838–9844 (2012).
17. C. Risko, M. D. McGehee, and J.-L. Bredas, "A quantum-chemical perspective into low optical-gap polymers for highly-efficient organic solar cells," *Chem. Sci.* **2**, 1200–1218 (2011).
18. P. Boland, K. Lee, and G. Namkoong, "Device optimization in PCPDTBT:PCBM plastic solar cells," *Sol. Energy Mater. Sol. Cells* **94**(5), 915–920 (2010).
19. J. Frenkel, "On the transformation of light into heat in solids. I," *Phys. Rev.* **37**, 17–44 (1931).
20. G. H. Wannier, "The structure of electronic excitation levels in insulating crystals," *Phys. Rev.* **52**, 191–197 (1937).
21. C. Crespo-Hernández, B. Cohen, and B. Kohler, "Base stacking controls excited-state dynamics in A·T DNA," *Nature* **436**, 1141–1144 (2005).
22. D. Markovitsi et al., "Molecular spectroscopy: complexity of excited-state dynamics in DNA," *Nature* **441**, E7 (2006).
23. I. Buchvarov et al., "Electronic energy delocalization and dissipation in single- and double-stranded DNA," *Proc. Natl. Acad. Sci. U. S. A.* **104**, 4794–4797 (2007).
24. T. Takaya et al., "UV excitation of single DNA and RNA strands produces high yields of exciplex states between two stacked bases," *Proc. Natl. Acad. Sci. U. S. A.* **105**, 10285–10290 (2008).
25. I. Vayá et al., "Fluorescence of natural DNA: from the femtosecond to the nanosecond time scales," *J. Am. Chem. Soc.* **132**, 11834–11835 (2010).
26. M. E. Casida, "Time-dependent density functional response theory for molecules," in *Recent Advances in Computational Chemistry*, D. P. Chong, Ed., Vol. **1**, pp. 155–192, World Scientific, Singapore (1995).
27. S. Tretiak, K. Igumenshchev, and V. Chernyak, "Exciton sizes of conducting polymers predicted by time-dependent density functional theory," *Phys. Rev. B* **71**, 033201 (2005).
28. K. I. Igumenshchev, S. Tretiak, and V. Y. Chernyak, "Excitonic effects in a time-dependent density functional theory," *J. Chem. Phys.* **127**(11), 114902 (2007).
29. L. Reining et al., "Excitonic effects in solids described by time-dependent density-functional theory," *Phys. Rev. Lett.* **88**, 066404 (2002).
30. A. Dreuw and M. Head-Gordon, "Single-reference ab initio methods for the calculation of excited states of large molecules," *Chem. Rev.* **105**, 4009–4037 (2005).
31. R. J. Magyar and S. Tretiak, "Dependence of spurious charge-transfer excited states on orbital exchange in TDDFT: large molecules and clusters," *J. Chem. Theory Comput.* **3**(3), 976–987 (2007).
32. A. J. Cohen, P. Mori-Sánchez, and W. Yang, "Insights into current limitations of density functional theory," *Science* **321**(5890), 792–794 (2008).
33. B. Kaduk, T. Kowalczyk, and T. Van Voorhis, "Constrained density functional theory," *Chem. Rev.* **112**(1), 321–370 (2012).

34. T. Ziegler and M. Krykunov, "On the calculation of charge transfer transitions with standard density functionals using constrained variational density functional theory," *J. Chem. Phys.* **133**, 074104 (2010).
35. S. Zheng, E. Geva, and B. D. Dunietz, "Solvated charge transfer states of functionalized anthracene and tetracyanoethylene dimers: a computational study based on a range separated hybrid functional and charge constrained self-consistent field with switching Gaussian polarized continuum models," *J. Chem. Theory Comput.* **9**, 1125–1131 (2013).
36. A. Dreuw and M. Head-Gordon, "Failure of time-dependent density functional theory for long-range charge-transfer excited states: the zincbacteriochlorin-bacteriochlorin and bacteriochlorophyll-spheroidene complexes," *J. Am. Chem. Soc.* **126**, 4007–4016 (2004).
37. R. Baer and D. Neuhauser, "Density functional theory with correct long-range asymptotic behavior," *Phys. Rev. Lett.* **94**, 043002 (2005).
38. D. P. T. Takeshi Yanai and N. C. Handy, "A new hybrid exchange-correlation functional using the Coulomb-attenuating method (CAM-B3LYP)," *Chem. Phys. Lett.* **393**, 51–57 (2004).
39. J.-D. Chai and M. Head-Gordon, "Systematic optimization of long-range corrected hybrid density functionals," *J. Chem. Phys.* **128**, 084106 (2008).
40. S. Refaely-Abramson et al., "Gap renormalization of molecular crystals from density-functional theory," *Phys. Rev. B* **88**, 081204 (2013).
41. Y. Park et al., "Tailored electronic structure and optical properties of conjugated systems through aggregates and dipole-dipole interactions," *ACS Appl. Mater. Interfaces* **5**, 4685–4695 (2013).
42. B. Mennucci et al., "Structures and properties of electronically excited chromophores in solution from the polarizable continuum model coupled to the time-dependent density functional theory," *J. Phys. Chem. A* **113**, 3009–3020 (2009).
43. J. A. Bjorgaard et al., "Solvent effects in time-dependent self-consistent field methods. I. Optical response calculations," *J. Chem. Phys.* **142**, 044103 (2015).
44. J. Tomasi, B. Mennucci, and R. Cammi, "Quantum mechanical continuum solvation models," *Chem. Rev.* **105**(8), 2999–3094 (2005).
45. B. Mennucci, "Polarizable continuum model," *Wiley Interdiscip. Rev. Comput. Stat.* **2**(3), 386–404 (2012).
46. C. A. Guido et al., "Electronic excitations in solution: the interplay between state specific approaches and a time-dependent density functional theory description," *J. Chem. Theory Comput.* **11**(12), 5782–5790 (2015).
47. R. Cammi et al., "Electronic excitation energies of molecules in solution: state specific and linear response methods for nonequilibrium continuum solvation models," *J. Chem. Phys.* **122**(10), 104513 (2005).
48. S. Corni et al., "Electronic excitation energies of molecules in solution within continuum solvation models: investigating the discrepancy between state-specific and linear-response methods," *J. Chem. Phys.* **123**(13), 134512 (2005).
49. R. Improta et al., "A state-specific polarizable continuum model time dependent density functional theory method for excited state calculations in solution," *J. Chem. Phys.* **125**, 054103 (2006).
50. R. Improta et al., "Toward effective and reliable fluorescence energies in solution by a new state specific polarizable continuum model time dependent density functional theory approach," *J. Chem. Phys.* **127**, 074504 (2007).
51. H. Li et al., "Comparison of LC-TDDFT and ADC(2) methods in computations of bright and charge transfer states in stacked oligothiophenes," *J. Chem. Theory Comput.* **10**(8), 3280–3289 (2014).
52. M. Lee, E. Geva, and B. Dunietz, "The effect of interfacial geometry on charge-transfer states in the phthalocyanine/fullerene organic photovoltaic system," *J. Phys. Chem. A* **120**, 2970–2975 (2016).
53. A. Austin et al., "A density functional with spherical atom dispersion terms," *J. Chem. Theory Comput.* **8**, 4989–5007 (2012).
54. S. Grimme, "Accurate description of van der Waals complexes by density functional theory including empirical corrections," *J. Comput. Chem.* **25**, 1463–1473 (2004).

55. S. Grimme, "Semiempirical GGA-type density functional constructed with a long-range dispersion correction," *J. Comput. Chem.* **27**, 1787–1799 (2006).
56. S. Grimme et al., "A consistent and accurate ab initio parametrization of density functional dispersion correction (DFT-D) for the 94 elements H-Pu," *J. Chem. Phys.* **132**, 154104 (2010).
57. Z. Zheng et al., "Effect of solid-state polarization on charge-transfer excitations and transport levels at organic interfaces from a screened range-separated hybrid functional," *J. Phys. Chem. Lett.* **8**(14), 3277–3283 (2017).
58. S. Zheng et al., "Ab initio study of the emissive charge-transfer states of solvated chromophore-functionalized silsesquioxanes," *J. Am. Chem. Soc.* **134**, 6944–6947 (2012).
59. R. Nieman et al., "The crucial role of a spacer material on the efficiency of charge transfer processes in organic donor-acceptor junction solar cells," *Nanoscale* **10**, 451–459 (2018).
60. J.-D. Chai and M. Head-Gordon, "Long-range corrected hybrid density functionals with damped atom-atom dispersion corrections," *Phys. Chem. Chem. Phys.* **10**, 6615–6620 (2008).
61. M. Cossi and V. Barone, "Time-dependent density functional theory for molecules in liquid solutions," *J. Chem. Phys.* **115**, 4708–4717 (2001).
62. M. J. Frisch et al., *Gaussian 09, Revision D.01*, Gaussian, Inc., Wallingford, Connecticut (2013).
63. F. Plasser and H. Lischka, "Analysis of excitonic and charge transfer interactions from quantum chemical calculations," *J. Chem. Theory Comput.* **8**, 2777–2789 (2012).
64. R. Martin, "Natural transition orbitals," *J. Chem. Phys.* **118**, 4775–4777 (2003).
65. S. Tretiak and S. Mukamel, "Density matrix analysis and simulation of electronic excitations in conjugated and aggregated molecules," *Chem. Rev.* **102**(9), 3171–3212 (2002).
66. H. Li et al., "Exciton scattering approach for optical spectra calculations in branched conjugated macromolecules," *Chem. Phys.* **481**(Suppl. C), 124–132 (2016).

Biographies for the authors are not available.